Geochemistry Geophysics Geosystems G3
AN ELECTRONIC JOURNAL OF THE EARTH SCIENCES
Published by AGU and the Geochemical Society

Article
Volume 7, Number 8
16 August 2006
Q08008, doi:10.1029/2005GC001209
ISSN: 1525-2027

Influence of rheology on realignment of mantle convective structure with plate motion after a plate reorganization

J. van Hunen
Institut für Geophysik, ETH Zurich, Schafmattstrasse 30, Zurich, CH-8093, Switzerland (hunen@erdw.ethz.ch)

S. Zhong
Department of Physics, University of Colorado at Boulder, Campus Box 390, Boulder, Colorado 80309-0390, USA (szhong@spice.colorado.edu)

[1] Small-scale convection (SSC) rolls below the oceanic lithosphere have the tendency to align with the large-scale shearing direction and thus with the plate motion direction relative to the deep mantle. Understanding the timescales of and processes responsible for realignment would contribute significantly to our understanding of the unresolved phenomena in the Pacific such as gravity lineations, small-scale seismic velocity variations, and intraplate volcanism that cannot be explained by hot spots. In this study we examine the evolution of those convection rolls when this relative plate motion direction is suddenly changed, as suggested by the kink in the Hawaii-Emperor seamount chain. Using three-dimensional numerical flow models, we investigate the realignment of SSC rolls after a change in plate motion direction. From the nature of the SSC, it is expected that rheological parameters dominate the characteristics of this realignment. Our results show that this is indeed the case. We find that (1) using constraints from onset timing of SSC, realignment of rolls can occur as fast as within 20 Ma, but might also take much longer, dependent on the rheology; (2) the realignment period is strongly correlated to the sum of large-scale shear stress induced by plate motion and small-scale shear stress from the SSC itself; (3) in a mantle deforming by dislocation creep, realignment occurs faster than by diffusion creep, because dislocation creep SSC is more vigorous; and (4) activation energy has little influence on the realignment time. Possible evidence for the realignment period might come from precise age determination of intraplate volcanism or azimuthal seismic anisotropy.

Components: 7889 words, 7 figures, 2 tables, 3 animations.

Keywords: alignment; convection rolls; plate motion; rheology.

Index Terms: 8020 Structural Geology: Mechanics, theory, and modeling; 8155 Tectonophysics: Plate motions: general (3040); 8160 Tectonophysics: Rheology: general (1236, 8032).

Received 1 December 2005; **Revised** 14 March 2006; **Accepted** 20 April 2006; **Published** 16 August 2006.

van Hunen, J., and S. Zhong (2006), Influence of rheology on realignment of mantle convective structure with plate motion after a plate reorganization, *Geochem. Geophys. Geosyst.*, *7*, Q08008, doi:10.1029/2005GC001209.

1. Introduction

[2] The dynamics of the mantle is dominated by instabilities of thermal boundary layers in various ways. Downwellings of cold, dense lithospheric plates in subduction zones and upwellings of plumes, probably from the core-mantle boundary, are the most obvious ones. On a smaller scale, convective instabilities in the bottom of the lithosphere form another type of boundary layer insta-

bilities, which are commonly described as sublithospheric small-scale convection (SSC) [*Richter*, 1973; *Richter and Parsons*, 1975; *Parsons and McKenzie*, 1978].

[3] Understanding of the physical process of SSC has been obtained through many laboratory and numerical studies, in which onset time and evolution of the subsequent lithospheric thinning and shallowing, and heat flow changes were studied [*Houseman and McKenzie*, 1982; *Davaille and Jaupart*, 1994; *Korenaga and Jordan*, 2003; *Huang et al.*, 2003; *Dumoulin et al.*, 2005; *Huang and Zhong*, 2005]. Figure 1 schematically illustrates the physics behind the development of a small-scale convective instability from a thermal boundary layer. Oceanic lithosphere on top of a hot (almost isothermal) upper mantle represents a gravitationally unstable situation. The top part of the lithosphere is very strong, which does not allow significant internal deformation. Only material at the bottom of the lithosphere with a viscosity up to $\sim$exp(2.24) $\approx$10 times that of the underlying mantle [*Davaille and Jaupart*, 1994] is weak enough to participate in a convective instability. As oceanic lithosphere cools and grows thicker, this weaker bottom layer of the lithosphere grows proportionally (the constant viscosity ratio η_t/η_b and therefore also the temperature ratio T_t/T_b between top and bottom of the SSC layer implies a constant ratio of $y_t/2\sqrt{\kappa t}$ over $y_b/2\sqrt{\kappa t}$, and therefore y_t/y_b is constant). When the local Rayleigh number of this layer exceeds the critical Rayleigh number, (small-scale) convection will start [*Howard*, 1964; *Davaille and Jaupart*, 1994; *Turcotte and Schubert*, 2002; *Dumoulin et al.*, 2005]. When a plate motion and background shearing are present, convection rolls aligning with the plate motions are gravitationally most unstable and will be the preferred orientation of SSC [*Richter*, 1973; *Marquart*, 2001; *van Hunen et al.*, 2003].

[4] Small-scale convection was first suggested as a process to explain the deviation of topography and heat flow of old oceanic seafloor from the theoretical purely conductive halfspace cooling predictions [*Parsons and McKenzie*, 1978; *Nagihara et al.*, 1996]. Gravity lineations in the Pacific were later attributed to the same process [*Haxby and Weissel*, 1986; *Buck and Parmentier*, 1986; *Marquart*, 2001]. Seismic tomographic observations suggest the presence of small-scale variations of seismic velocities below the old Pacific [*Katzman et al.*, 1998], and present evidence for a "reheating phase"

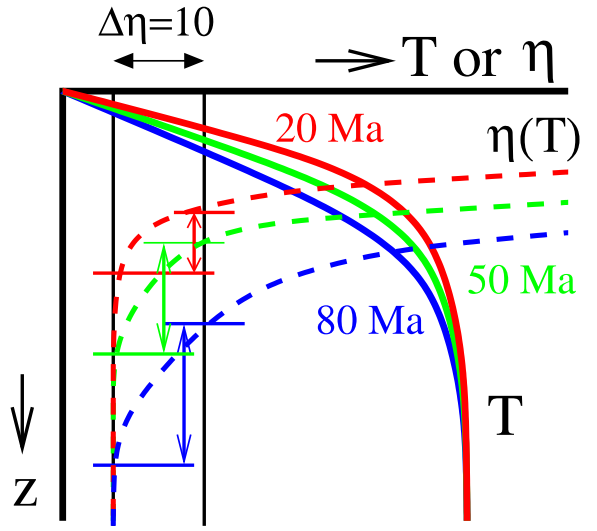

Figure 1. Illustration of SSC roll formation. Only the bottom part of the lithosphere with a viscosity less than 10 times the underlying mantle will eventually participate in convection. This layer grows proportional to the total lithospheric thickness the local Ra exceeds the critical Rayleigh number until thick enough to form convection.

of the Pacific lithosphere between 70 and 100 Ma [*Ritzwoller et al.*, 2004]. It has furthermore been suggested that SSC is a mechanism to create intraplate volcanism that cannot be attributed to hot spot volcanism [*Haxby and Weissel*, 1986; *Doin and Fleitout*, 1996; *Raddick et al.*, 2002]. Gravity lineations, seismic tomography patterns, and volcanic alignments all occur in elongated structure that, to some extend, align with the present-day Pacific plate motion. If these processes are indeed the result of SSC, then orientation relative to the plate motion direction should tell us something about the response of SSC to changes in plate motions.

[5] The bend in the Hawaii-Emperor chain of seamounts (HEB) is dated at 43–47 Ma. It forms the classical example of a sudden change in the relative motion between the Pacific lithosphere and the underlying Hawaiian mantle plume [*Morgan*, 1971]. *Richter* [1973] and *Richter and Parsons* [1975] showed the dominance of longitudinal convection rolls of mantle flow below a lithosphere that moves with respect to the deeper mantle as a result of shearing between the lithosphere and the deeper mantle. On the basis of laboratory studies of isoviscous fluid flow they suggested that within 20–50 Ma rolls would align with the plate motion if the plate moves with 10 cm/yr [*Richter and Parsons*, 1975]. This implies that by now, 43–47 Ma after

the major change in Pacific plate motion direction, SSC roll structures would have aligned again with the plate motion. The importance of these results lies in the guidance of any search for observational evidence for SSC structures: it tells us what kind of structures we can expect.

[6] In this study, we further elaborate on this pioneering work. In particular, we are interested in the role of more sophisticated Earth-like rheology on the development and realignment of SSC roll structures with a changing plate motion. This issue was not addresses in the early work of Richter, but is likely to play a dominant role, because the appearance of SSC in itself is dominated by rheological parameters. We will address the following questions. Do preexisting SSC rolls influence the development of newly oriented rolls after a change in plate motion direction? What are the influences of rheological parameters (diffusion vs. dislocation creep, activation energy, rheological layering, effective mantle viscosity) on the style and timescale of the realignment of the roll structures with the new plate motion direction? What are the possible observations to further constrain our model results? The paper is organized as follows. After presenting the governing equations and modeling techniques, we discuss the modeling results on the basis of a few key results. Next, we will present a method to quantify the dominant roll structure through time. This quantification of the results enables us to draw some general conclusions. Finally we discuss the implications and observations of the results.

2. Methods, Model Description, and Techniques

[7] Calculations are performed with a three-dimensional (3-D) finite element code Citcom [*Moresi and Gurnis*, 1996; *Zhong et al.*, 2000], extended for nonlinear (stress dependent) rheology [*van Hunen et al.*, 2005]. Fluid flow is incompressible, has infinite Prandtl number, adopts the Boussinesq approximations [e.g., *Schubert et al.*, 2001], and is governed by the following nondimensional equations [*McKenzie et al.*, 1974]:

$$\nabla \cdot \mathbf{u} = 0, \tag{1}$$

$$-\nabla P + \nabla \cdot \left[\eta\left(\nabla \mathbf{u} + \nabla^T \mathbf{u}\right)\right] + \mathrm{Ra} T \mathbf{e}_z = 0, \tag{2}$$

$$\frac{\partial T}{\partial t} + \mathbf{u} \cdot \nabla T = \nabla^2 T. \tag{3}$$

These equations describe the conservation of mass, momentum and thermal energy, respectively. Symbols are described in Table 1, and in our (bottom-heated) experiments the Rayleigh number *Ra* is defined in the usual way:

$$\mathrm{Ra} = \frac{\alpha \rho_0 g \Delta T h^3}{\kappa \eta_0}. \tag{4}$$

Equations (1) to (3) are nondimensionalized in the following way: $\mathbf{x}^* = \mathbf{x}'h$, $t^* = t' h^2/\kappa$, $\eta^* = \eta' \eta_0$, and $T^* = T' \Delta T$. The primes are dropped in equations (1) to (3) and the remainder of the paper for clarity.

[8] A general nonlinear rheology is implemented:

$$\dot{\epsilon} = A\sigma^n \exp(-E^*/RT_{\mathrm{abs}}), \tag{5}$$

which is benchmarked against results from *Christensen* [1984]. This enables us to use both diffusion creep (with $n = 1$) and dislocation creep (for which we took $n = 3.5$ [*Karato and Wu*, 1993]). The prefactor A is chosen such that the effective viscosity $\eta_{\mathrm{eff}} = \sigma/\dot{\epsilon} = \eta_0$ at mantle temperature (i.e., nondimensional temperature $T = 1$) and, in the strain-rate dependent viscosity case $n > 1$, under stress/strain rate conditions that result from the imposed velocity at the inflow boundary. We constrain η_{eff} (and therefore also A) with SSC onset times rather than with laboratory measurements, because the effective mantle viscosity is not very accurately known due to the uncertainties in, e.g., the amount of hydration.

[9] Calculations are performed in a rectangular box of 14,000 by 2000 or 4000 km wide and 670 km deep, representing a part of the western Pacific oceanic upper mantle. All calculations have a $T = 1350$°C and no-slip conditions as bottom thermal and flow boundary conditions. At the surface, $T = 0$°C and a plate motion of 8.6 cm/yr is prescribed with respect to the bottom boundary in the direction of increasing x coordinate. The combination of prescribed plate motion and a no-slip bottom boundary condition produces the shear that is responsible for the alignment of convective rolls with the plate velocity. The front and back side boundaries (at minimum and maximum y coordinate, respectively) have symmetry boundary conditions for both the momentum and energy equations ($v = \sigma_{xy} = \sigma_{yz} = dT/dy = 0$). Such boundary conditions are common for convection simulations, and although in this specific case of oblique convection rolls these boundary conditions are not ideal, they probably still are the least restrictive ones to the flow. By making the calcu-

Table 1. Symbols and Model Parameters

Symbol	Description	Value/Dimensions
A	rheological prefactor	$Pa^{-n}\ s^{-1}$
C	gradient structure tensor	-
E^*	activation energy	$kJ\ mol^{-1}$
$\mathbf{e}_z$	unit vector in vertical direction	-
h	vertical model size	670 km
g	gravitational acceleration	$9.8\ m/s^2$
n	rheological exponent	-
P	pressure	-
R	gas constant	8.3 J/mol, K
Ra	Rayleigh number	-
T	temperature	-
T_0	surface temperature	273 K
T_{abs}	absolute temperature = $T^*\Delta\ T + T_0$	K
t	time	-
$\mathbf{u}$	= {u, v, w}, velocity	-
v_{pl}	plate velocity	cm/yr
$\mathbf{x}$	= {x, y, z}, spacial coordinates	-
$z_{\Delta\eta}$	depth of rheological layering	-
α	thermal expansion coefficient	$3.5 \times 10^{-5}\ K^{-1}$
β	dominant roll structure angle with plate motion direction	-
$\Delta\eta$	viscosity jump at depth $z\Delta\ \eta$	-
ΔT	temperature drop over model	1350 K
$\dot{\epsilon}$	2nd invariant of strain rate	s^{-1}
$\dot{\epsilon}_{SSC}$	small-scale $\dot{\epsilon}$ by SSC	s^{-1}
$\dot{\epsilon}_{pl}$	large-scale $\dot{\epsilon}$ by v_{pl}	s^{-1}
η	viscosity	-
η_0	reference viscosity	Pa s
η_{asth}	asthenospheric viscosity (minimum horizontally averaged effective viscosity)	Pa s
η_{eff}	effective viscosity	Pa s
κ	thermal diffusivity	$10^{-6}\ m^2/s$
ρ_0	reference density	$3300\ kg/m^3$
σ_{ij}	stress tensor	Pa
σ	2nd invariant of stress	Pa

lations in the restart phase 4000 km wide, we ensure little effect of the boundary conditions on the interior of the box. The inflow temperature field corresponds to either a half-space cooling model for 5 Ma old lithosphere (for the "initial phase" described below) or a numerically interpolated field from this "initial phase" (for the "restart phase", also described below). At in- and outflow boundaries, a horizontal flow-through velocity boundary condition is imposed to simulate large-scale Couette-type flow resulting from plate motion relative to the deep mantle: the velocity field is normal to the inflow boundary (no components in y and z direction) and the shear between the top and bottom of the box is distributed such that the horizontal shear stress $\sigma_{xz} = \dot{\epsilon}_{xz}\eta_{eff}$ is constant for each column of elements on the inflow boundary: $v_x(z) = v_{pl} - \int_{z'=0}^{z} \dot{\epsilon}_{xz}(z')dz'$. This flow condition is copied onto the opposite boundary as the outflow boundary condition. This outflow boundary is put far away of the region of interest, such that the influence on the flow pattern in the box's interior is negligibly small.

[10] All results share the same three-phase modeling procedure: (1) an "initial" flow phase for given plate motion direction is followed by (2) a sudden event of rotation of the plate motion direction, after which (3) a second "restart" phase is started. Figure 2 illustrates this procedure using the model results of model Case 1 (which is described in detail in Table 2).

[11] 1. In the initial phase, time integration of the flow and temperature distribution inside the model domain is performed until a statistically steady state thermal solution is obtained.

[12] 2. Second, the temperature solution is mirrored several times in the y direction, i.e., the direction perpendicular to the plate motion direction. In this way a solution in a wider domain is obtained, from which a box with a 60 degree

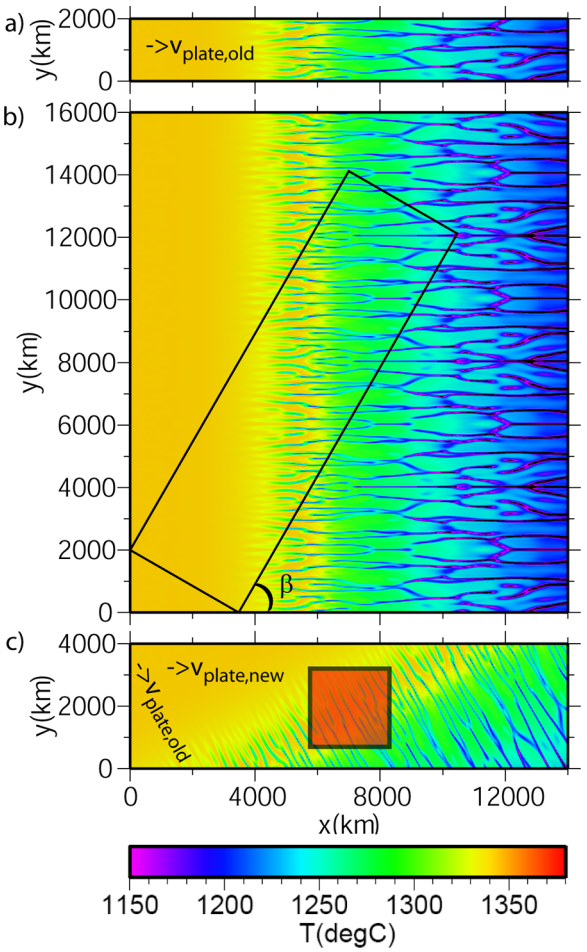

Figure 2. Modeling technique to simulate a sudden change in the plate motion direction, illustrated with a horizontal cross section at 150 km depth of the temperature field for Case 1. (a) An initial calculation is performed until thermal statistical steady state solution is obtained. (b) Mirroring the temperature field several times in the y direction provides a wide solution. A box of 14000 $\times$ 4000 km with $\beta = 60^\circ$ with the x axis is cut out. (c) The resulting temperature field is used as initial and boundary conditions in a restart calculation. The red box indicates the surface area below which the dominant roll structure is quantified. Different initial locations for this rectangle are used, and the rectangle moves along with the lithospheric plate.

azimuthal clockwise rotation with respect to the original calculation is cut out. This rotation represents a sudden change in the plate motion direction with respect to the deep mantle or hot spot reference frame, and can be related to the kink in the Hawaii-Emperor seamount chain.

[13] 3. During the restart phase, a new calculation is started from this rotated box to examine the effect of this sudden change in plate motion direction on the development convective structure.

[14] Such three phase procedure is equivalent to producing a single model calculation in which the plate motion is suddenly changed, but this approach is computationally more efficient and technically more feasible. During the restart phase, the inflow temperature distribution effectively represents a MOR oblique to the spreading velocity, such as modeled by *Morency et al.* [2005], although the MOR is not explicitly present in our model. Technically, the differences between the initial and the restart phases are the numerical resolution, the initial and inflow boundary conditions for the temperature field, and the lateral size of the box in plate-motion-perpendicular direction. Initial phase calculations are performed in a 2000 km wide box, which is wide enough to avoid any side boundary effects [*van Hunen et al.*, 2005], and each calculation is performed with 256 $\times$ 64 $\times$ 24 elements. For the restart phase, a 4000 km wide box is used to ensure that also in this case, where structures oblique to the side walls are more dominant, the box is wide enough. In that case, the numerical resolution in x direction is taken equal to that in y direction to accurately resolve roll structures oblique to the plate motion, and those calculations are thus performed with 512 $\times$ 128 $\times$ 24 elements. We apply vertical mesh refinement in the top half of the box to increase the resolution there. One calculation with small length scales for thermal structure (Case 2, Table 2) was recalculated with 1.5 times more elements in each horizontal direction to check for sufficient spatial resolution.

[15] The applied version of Citcom uses a parallel full-multigrid iterative solver [*Moresi and Solomatov*, 1995; *Moresi and Gurnis*, 1996; *Zhong et al.*, 2000] for the Stokes equation (equations (1) and (2)), and a SUPG explicit solver [*Brooks and Hughes*, 1982] to obtain the temperature field. Parallel calculation is performed using domain-decomposition with MPI [*Zhong et al.*, 2000].

[16] Apart from visual inspection, the SSC onset time and dominant convective roll structure orientation can be obtained more quantitatively and objectively. Onset time of SSC is taken as the lithospheric age where the thermal field for the first time deviates more than 1% from the cooling halfspace solution [*Davaille and Jaupart*, 1994]. In some cases, minor fluctuations in the temperature field can be observed prior to this onset time. For the roll structure orientation, we use a method

Table 2. Model Calculations and Their Model Parameters

Case	n	E^*, kJ/mol	Ra, $\times 10^7$	v_{pl}, cm/yr	η_{asth},[a] $\times 10^{19}$ Pa s	$\Delta\eta$,	$z_{\Delta\eta}$, km	$\dot{\epsilon}_{pl}$, $\times 10^{-15}$ 1/s	$\dot{\epsilon}_{SSC}$, $\times 10^{-15}$ 1/s	t_{2000},[b] Ma	t_{4000},[b] Ma	t_{6000},[b] Ma
1	1.	120.	1.2	8.6	4.86	50.	400.	9.1	3.6	43.	35.	27.
2	3.5	360.	2.4	8.6	1.38	50.	400.	9.1	15.	18.	16.	15.
3	1.	120.	1.2	8.6	4.29	-	-	4.8	3.6	83.	73.	62.
4	1.	120.	1.2	8.6	5.52	50.	300.	13.6	3.6	17.	21.	17.
5	1.	120.	1.2	4.0	4.86	50.	400.	4.2	3.6	90.	83.	63.
6	1.	360.	3.9	8.6	1.60	50.	400.	9.1	3.8	44.	34.	27.
7	1.	120.	3.0	8.6	2.54	50.	400.	9.1	5.7	33.	26.	25.
8	3.5	540.	3.9	8.6	0.99	50.	400.	9.1	19.	15.	17.	17.
9	3.5	360.	3.2	8.6	1.28	50.	400.	9.1	22.	18.	13.	12.
10	3.5	360.	2.1	8.6	1.55	-	-	4.8	14.	27.	23.	21.

[a] The asthenospheric viscosity η_{asth} is defined as the minimum, horizontally averaged effective viscosity at the beginning of the restart phase.
[b] Characteristic realignment time t (Ma) is defined in the text.

described as the multi-scale principal components analysis of local orientation [*Feng and Milanfar*, 2002; *Rieger and van Vliet*, 2003]. It uses the concept that the roll orientation is perpendicular to the direction of the largest average horizontal thermal gradient. This means that the orientation of the dominant roll structures is represented by the eigenvector corresponding to the smallest eigenvalue of the gradient structure tensor

$$C = \overline{\nabla T \nabla T}^t, \tag{6}$$

where the bar represents the average over a local volume. Here, this local volume is defined as the volume of the top 200 km below an approximately square surface area of 2400 × 2400 km, as indicated by the red area in the cross section in Figure 2c. This surface area is chosen rather arbitrarily, but it is large enough to ensure observing the "global" behavior rather than that of an individual SSC roll, but small enough to avoid mixing lithosphere of completely different ages. This region moves along with the lithospheric plate, and different starting positions were examined.

[17] The presented model setup is chosen such that sublithospheric SSC can be studied efficiently. However, a second, much smaller thermal boundary layer develops at the bottom of the model, from which instabilities in the form of small hot plumes may arise, as indicated in a cross section of the thermal field in a previous paper [*van Hunen et al.*, 2005]. These plumes do not seem to influence the planform an vigor of SSC significantly.

3. Model Results

[18] The development of roll structures after a change in the plate motion direction is illustrated in Figure 3. Table 2 describes the model parameters

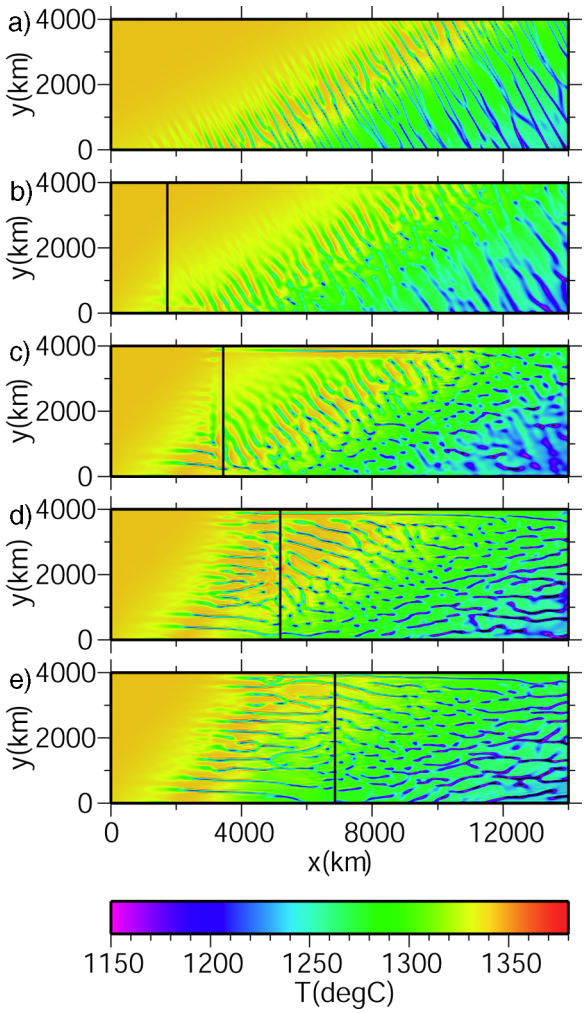

Figure 3. Thermal field at 150 km depth to indicate the development of roll structure in the default case (Case 1, see Table 2). (a) Initial situation at time of restart (t = 0). (b and c) After 20 and 40 Ma, the old roll structure is still dominating. (d and e) Only after 60 Ma, new roll structure clearly starts to overprint the old one, which seems completed at 80 Ma. A depiction of this process is available as Animation 1.

for this model (Case 1) and other models. In this first case, a Newtonian rheology ($n = 1$) with rather low activation energy $E^* = 120$ kJ/mol, a plate motion of 8.6 cm/yr, $Ra = 1.2 \times 10^7$, and a rheological layering at 400 km depth with a 50-fold jump in the effective viscosity were used. Such low activation energy mimics the effect of dislocation creep with a Newtonian fluid [*Christensen*, 1984]. The 50-fold jump in viscosity at 400 km depth is motivated by *Hager and Richards* [1989] results from geoid constraints, and results in almost complete concentration of the shear induced by plate motion in the upper 400 km, and the actual size of the viscosity jump has little influence in this case. These parameter settings give small-scale convection with an onset time of approximately 70 Ma, and its reheating effects were shown to fit seismic surface wave observations [*van Hunen et al.*, 2005]. After the rotation event, described above, Figure 3a shows a horizontal cross section at the beginning of the restart phase at 150 km depth (where for this calculation SSC rolls are most pronounced). It clearly illustrates the orientation of the "old" roll structures relative to the new orientation of the box and the plate motion direction. Figures 3b, 3c, 3d, and 3e show the resulting SSC roll pattern development after 20, 40, 60 and 80 Ma, respectively, of time integration with a left-to-right plate motion direction (i.e., in the direction of increasing x coordinate). The vertical solid line in those plots indicates the divide between the "old" part (the part which previously experienced the old plate motion direction), and the "new" lithosphere (that was flowing into the model domain only after the rotation in plate motion direction had occurred). Since no "memory" of old roll structures exists in the new part, it is not surprising that convective rolls align with the new plate motion there, similar to the initial-phase roll structures before the change in plate motion direction. Unlike before the rotation phase, the line where initial SSC occurs (or "SSC front") is not perpendicular to the plate motion anymore after rotation, and a thermal gradient remains in the plate-motion-perpendicular direction. This is because the lithospheric age at the inflow boundary, inherited from the rotated initial calculation, is kept as the thermal boundary condition throughout the whole restart calculation. In the old part, we see that after 20 Ma the old structure is still clearly present, although thermal gradients have smoothed somewhat. After 40 Ma, roll structures below the oldest part of the plate show a realignment, and rolls parallel to the plate motion start to appear. After 60 Ma, most old rolls have disappeared and have been replaced by rolls parallel

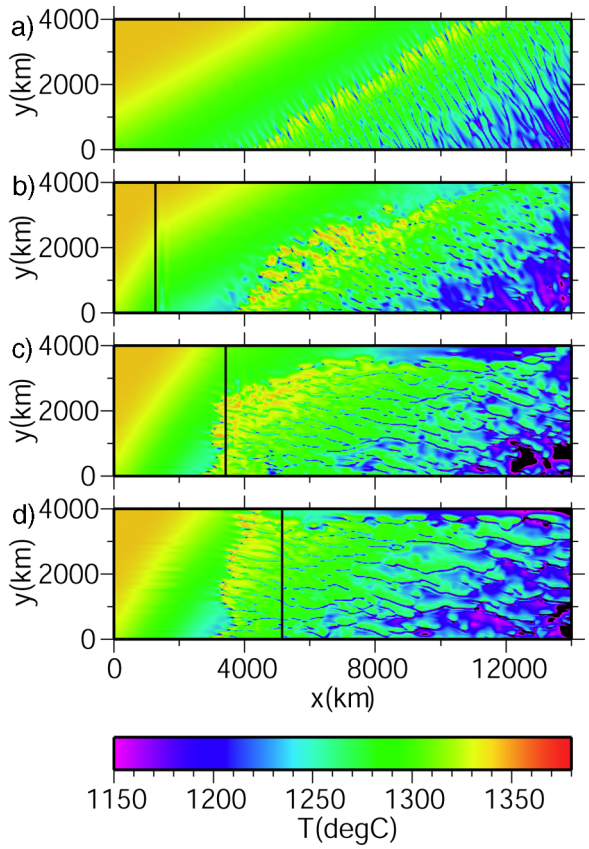

Figure 4. (a–d) As Figure 3, but for Case 2: $n = 3.5$, $E^* = 360$ kJ/mol. Cross sections are taken at a depth of 120 km. (b) Already after 20 Ma, old structures have been significantly overprinted. (c and d) After 40 Ma, the dominant angle β between the roll structures and the plate motion direction remains constant at about 10–20°. A depiction of this process is available as Animation 2.

to the plate motion, and after 80 Ma roll alignment with the new plate motion seems complete. From this we can conclude that for this case, roll realignment with the plate motion occurs within 60 to 80 Ma Animations 1.

[19] Case 2 shows the same type of calculation with a different rheology: $n = 3.5$, $E^* = 360$ kJ/mol, and $Ra = 2.4 \times 10^7$. Results are shown in Figure 4. As with Case 1, also this parameter combination gives small-scale convection below lithosphere of ~70 Ma, and its lithospheric reheating effect fits the seismic observations [*van Hunen et al.*, 2005]. After the rotation event, a temperature field is obtained again which has roll structures oblique to the new plate motion direction. A cross section at 120 km depth of this field is shown in Figure 4a. Roll-structures are somewhat finer (i.e., on a smaller scale), but otherwise comparable to

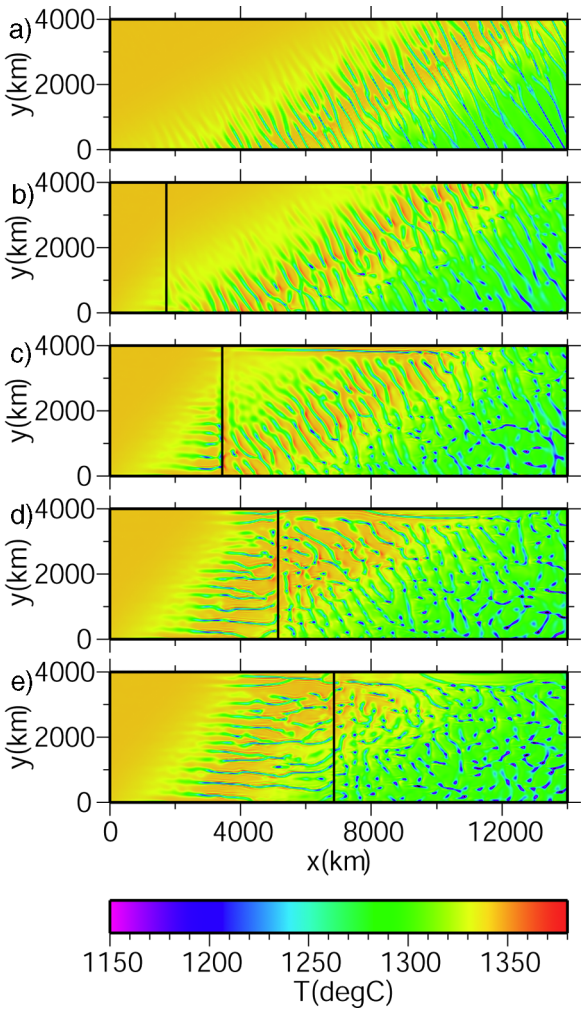

Figure 5. Horizontal cross section of the temperature field at 150 km depth. As Figure 3, but for Case 3: $\Delta\eta = 1$. During the full 80 Ma of model calculation, rolls do not clearly align with the new plate motion. Instead, dot structures indicate plume like downwellings, and transverse roll structures perpendicular to the plate motion are visible. A depiction of this process is available as Animation 3.

the ones in Figure 3. After starting the restart phase, old structures are quickly erased: after already 20–30 Ma, the old plate motion direction cannot be easily recognized anymore. Later, a small angle between the rolls and the plate motion direction remains, which is probably due to the age variation of the plate in y direction. For these rheological settings, realignment of the rolls with the plate motion is completed in about 20–30 Ma: much faster than for the Newtonian case-1 calculation. After 60 Ma the front of the SSC region is not as strongly correlated to the age of the plate as in Case 1: in general, onset age of SSC in case of nonlinear rheology fluctuates significantly, due to complicated feedback between (large- and small-scale) shearing, thermal erosion, and the effective viscosity Animation 2.

[20] Case 3 is illustrated in Figure 5. In this case, we again adopted the Newtonian rheology settings from case 1, but removed the rheological boundary at 400 km depth. In Case 1 the shearing between the plate motion and the deeper mantle was mainly confined to the upper mantle above 400 km depth, as the mantle below is much stiffer and shears much less. Removing the rheologically strong layer below 400 km depth spreads out the shearing between the moving plate and the deep mantle over a larger depth range, and thus reduces the shear stress. Since this shearing is responsible for the alignment of SSC rolls with the plate motion, we expect this reduced shearing to lead to reduced realignment. Figure 5 shows that this is indeed the case. Even after 60 Ma, the old roll structures can still be recognized. Even where old roll structure is overprinted, a clear pattern of new rolls aligning with the plate motion is not visible. Instead, isolated dots in Figures 5c–5e indicate the presence of plume like downwellings without a clear orientation. Note that simultaneously below the "new" plate roll structures are forming: this clearly indicates that the presence of old structure severely hampers the formation of new structure. Figure 5 shows that shearing plays a dominant role in the alignment of rolls with plate motion Animation 3.

[21] We performed several more calculations, and all model parameters are given in Table 2. We quantified the dominant orientation of the roll structure in all models using the eigenvectors from the average thermal gradient structure tensor in a local area. Figure 6 shows the resulting dominant realignment angle β for each calculation inside the local area as a function of elapsed model time since the plate motion rotation. The left edge of the calculation rectangle (shown in Figure 2c) was initially positioned at 2000 km (Figure 6a), 4000 km (Figure 6b), or 6000 km (Figure 6c) from the inflow boundary. In all cases, the rectangle moves along with the lithospheric plate (i.e., toward the right). Figure 6a therefore follows the structure development for a fairly young lithospheric plate, whereas Figure 6c shows results for an older lithosphere. Although those three sets of results are qualitatively similar, rotation timescales are shorter for older parts of the lithosphere (Figure 6c) than for younger parts (Figure 6a). Case 1 shows a rather constant angle of >50° for

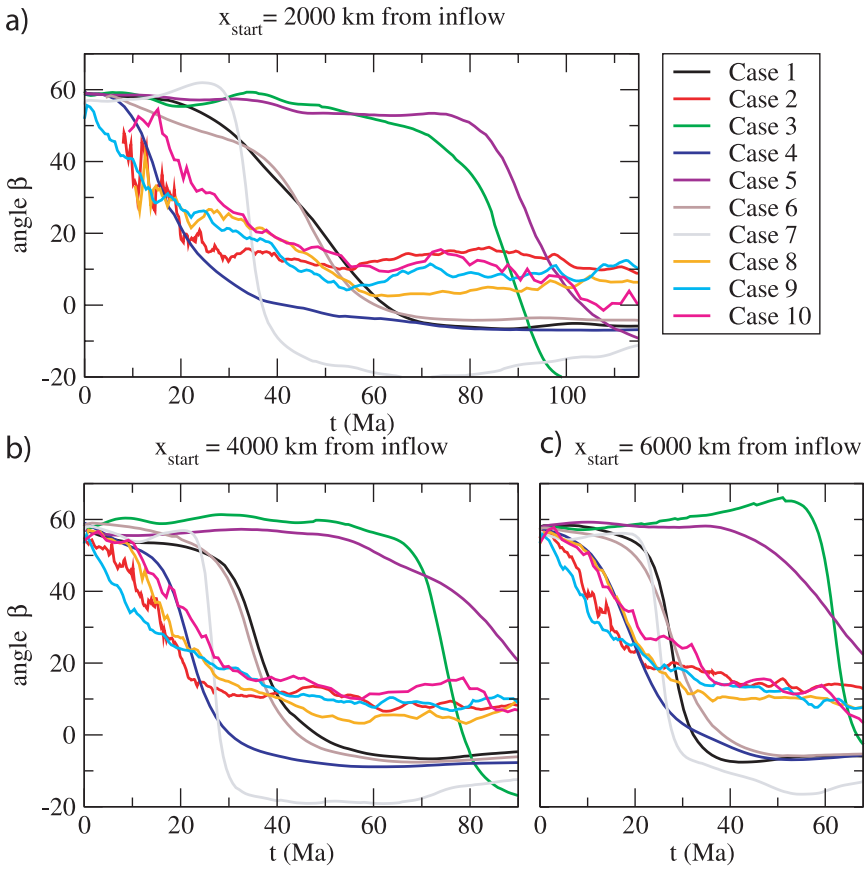

Figure 6. Dominant roll angle β of the roll structures with respect to the new plate motion direction in the red rectangular area shown in Figure 2c. In all calculations, the rectangle moved along with the plate. The initial location of the left edge of the rectangle was located at (a) 2000 km, (b) 4000 km, and (c) 6000 km from the inflow boundary. Model parameters are described in Table 2. See text for method description of the calculation of β.

the first 20 Ma. This corresponds to the initial angle of 60° imposed by the rotation. After that, a gradual decrease of the dominant angle sets in, which reaches a new equilibrium value around 0° after about 30–60 Ma, depending on the part of the lithosphere for which the calculations are performed. As also shown in Figure 4, the case with nonlinear rheology changes its dominant roll angle much quicker: decrease of that angle sets in immediately after the plate motion rotation, and reaches 10° in about 25 Ma. After that the angle does not decrease any further. Case 3 shows no significant angle decrease in the first 50–60 Ma. After that, a change in orientation toward 0° also occurs in this case.

[22] Seven more cases (four with Newtonian rheology, and three with non-Newtonian rheology) are shown in Figures 6a–6c. Case 4 has increased shearing, because the shearing zone is confined to the depth range between the bottom of the lithosphere and 300 km depth instead of 400. This results in a faster realignment of the rolls with the new plate motion. Case 5 has a reduced plate velocity, and therefore also a reduced shearing, similar to Case 3. Also the realignment is slower than in the default Case 1, as expected. An increased activation energy in Case 6 from 120 to 360 kJ/mol has no significant effect on the realignment time. This is rather surprising given the fact that the activation energy plays such a dominant role in the vigor and amount of small-scale convection [*Davaille and Jaupart*, 1994; *Solomatov*, 1995; *Choblet and Sotin*, 2000; *Huang et al.*, 2003; *Korenaga and Jordan*, 2003; *van Hunen et al.*, 2005]. All the previous cases had approximately similar SSC onset times of around 70 Ma. In Case 7, we reduced the SSC onset time (measured in the initial phase) to about 35 Ma by decreasing the effective mantle viscosity (and thus increasing Ra)(Case 7). This case shows the same initial period of little change in angle β, but after this period, alignment with the new plate motion direction is significantly faster. Case 8 is similar to the

non-Newtonian rheology Case 2, but the activation energy is increased from 360 kJ/mol to 540 kJ/mol. Ra is increased as well to keep the SSC onset time comparable to Cases 1–6. Figure 6a shows very little difference with Case 2, and Figures 6b and 6c show a small delay in the realignment compared to Case 2. Case 9 is again comparable to Case 2, but has a smaller SSC onset time of about 35 Ma. Figure 6a shows that realignment is very little affected by this change, and Figures 6b and 6c show a slightly earlier realignment compared to Case 2. In the final Case 10, we removed the rheological boundary at 400 km depth, and extended the upper mantle rheology down to 670 km depth, similar to Case 3, but for non-Newtonian rheology. The effect is also comparable to Case 3, but less dramatic: realignment is delayed in all cases shown in Figures 6a–6c.

4. Discussion

[23] The results suggest that shearing and type of rheology both play an important role in the realignment period. We investigate these results here in some more detail. As a first-order estimate, the strain rate produced by the plate motion with respect to the deep mantle can be estimated by dividing the plate speed by the thickness of the shear layer. This shear layer extends from approximately 100 km depth (the typical depth of the bottom of the lithosphere in all calculations) to the depth of the rheological boundary at 300 or 400 km depth, or, if this boundary is absent, to the bottom of the model domain at 670 km depth. Results are given in Table 2 as $\dot{\epsilon}_{pl}$. Another type of shearing is created by the SSC itself. Although the orientation of this shearing is not uniform as with shearing due to the large-scale plate motion, this strain rate might still affect the realignment period in some way. *Solomatov and Moresi* [2000] provide an estimate for the SSC velocity (their equation (28)). By dividing this velocity by the typical length scale of the SSC convection cells, we obtain a typical strain rate produced in the SSC cells. Although this SSC length scale differs somewhat from case to case, we decided to use 200 km as a typical value. Results are given in Table 2 as $\dot{\epsilon}_{SSC}$. We estimate the total strain rate from both plate motion and SSC motion by simply adding the two strain rates. We quantify the relation between this total strain rate and the characteristic realignment time in Figure 7. Here we defined this characteristic realignment time as the time it takes for the angle β to reach 30 degrees (i.e., halfway between the old and the new plate motion direction angle). These values are added to Table 2 as t_{2000}, t_{4000}, and t_{6000} for results from Figures 6a–6c, respectively. The different colors in Figure 7 represent results from Figures 6a–6c. The correlation is rather good, given the intrinsic randomness of the SSC process [*Huang et al.*, 2003], and both Newtonian and non-Newtonian results have the same correlation between realignment period and total strain rate.

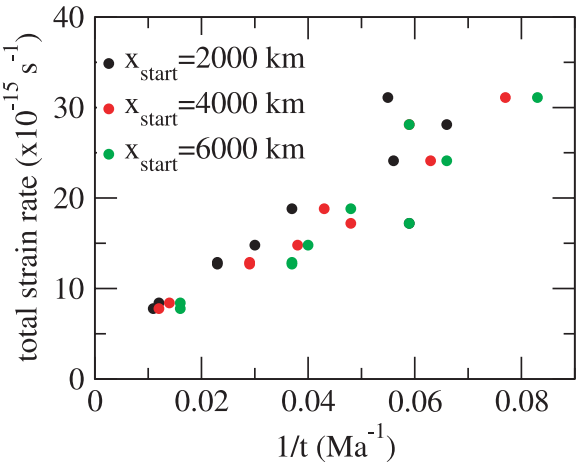

Figure 7. Correlation of the characteristic realignment period (see text) with the total shear as a result of plate motion and SSC. Different colors refer to different initial location of the red rectangular in Figure 2c at 2000, 4000, and 6000 km from the inflow boundary. Characteristic realignment periods are measured from Figures 6a–6c and are given in Table 2.

[24] Figures 6a–6c show that rotation of the dominant structures toward the new plate motion does not occur in the same way for all shown calculations. We might be able to split the total "realignment period" (the period needed from rotation to complete alignment with the new plate motion direction) into an initial "delay period" (in which the dominant angle β remains more or less constant), and a "rotation period" (which describes the rather rapid decrease of angle β, and thus the actual rotation of the dominant structures). Note that the characteristic realignment time defined above represents some average of the total realignment period and the delay period. Some cases have a long delay period: they keep their initial angle close to 60° for a long period of time (Cases 3 and 5) before significant rotation occurs. Other cases (Cases 2, 4, and 8–10) start rotating almost immediately after the change in plate motion direction. There seems to be a relationship between the large-scale shear strain rate due to plate motion

and this delay period: Case 3 has a more distributed shear, and Case 5 has less shear due to a slower plate motion, while Case 4 has all shear concentrated in a shallow layer below the lithosphere. The reason for the absence of this delay period in the case with nonlinear rheology (Cases 2, and 8–10) is related to the large SSC shearing of those cases. The rotation period is completed in 10 Ma for most calculations.

[25] The activation energy E^* plays an important role in the development of SSC [e.g., *Huang et al.*, 2003; *van Hunen et al.*, 2005]. It may therefore be surprising to see that the influence of E^* on the realignment period is very small. This realignment period is predominantly influenced by the local amount of shearing. Both the large-scale plate-induced shearing and the shearing by SSC are independent of E^*. Large-scale shearing only depends on v_{pl} and the depth of asthenosphere, while in case of small-scale shearing, E^* is almost completely balanced by a similar change in the appropriate Rayleigh number [*Solomatov and Moresi*, 2000] to keep the onset time unchanged. Timescales for realignment are shorter for older parts of the plate (compare Figures 6a–6c). One reason for that probably is that the thicker old lithosphere reduces the thickness of the underlying asthenosphere, and therefore increases the local large-scale strain rate. Figure 6 also shows that after rotation, not all angles approach $\beta = 0°$: the nonlinear rheology Cases 2, and 8–10 only reaches 10–20°, and does not decrease any further, while Cases 3 and 7 have their angle β drop to values as low as −20°. All these Cases have a relatively large $\dot{\epsilon}_{SSC}$ to $\dot{\epsilon}_{pl}$ ratio, which indicates that the more dominant the shearing by plate motion is compared to shearing by SSC, the better the realignment with the new plate motion direction (and the smaller the absolute value of β). The deviation of realignment angle from its expected value $\beta = 0°$ is most likely related to the laterally varying age of the inflowing plate in the restart phase. This age variation is partly the result of the present model setup, and gives rise to large-scale nonzero lithospheric thickness variations and mantle flow components in the direction perpendicular to the plate motion direction. However, such plate thickness variation and mantle flow perpendicular to the plate motion might be present in the Pacific as well to some extent, and a perfect $\beta = 0°$ should perhaps not be expected.

[26] Recently, the debate on the fixity of hot spots has been refueled by evidence for southward motion of the Hawaiian hot spot until 43–47 Ma [*Tarduno et al.*, 2003; *Steinberger et al.*, 2004]. The similarity of the shapes of the Hawaiian and Louisville hot spots suggests, that if the plume locations were moving south in the past, it must have been occurring on a large scale [*Tarduno et al.*, 2003], and probably involved a southward motion of the local lower mantle. Concerning upper mantle shearing direction (which determines the SSC roll development and orientation), there is no difference between the Pacific plate ceasing to move North or the lower mantle (including the mantle plumes) ceasing to move South at around 43–47 Ma, because only the relative motion between the Pacific plate and the deep mantle is responsible for the shearing. Therefore our results may be valid for either the case of southward motion of Hawaii and Louisville or northward motion of the Pacific plate.

[27] Our present knowledge of the rheological conditions in the Pacific upper mantle may not be accurate enough to distinguish between the presented rheological models. Therefore future observations of mantle structure below Pacific lithosphere older than 43–47 Ma may give us valuable information. Chains of intraplate volcanism may help us in this case, because their origin might be related to small-scale convection underneath [*Haxby and Weissel*, 1986; *Doin and Fleitout*, 1996; *Raddick et al.*, 2002]. Some seamount chains such as Puka Puka and Crossgrain Ridges [*Lynch*, 1999], seamounts between Ducie Island and the Easter microplate [*Searle et al.*, 1995] or the Sojourn Ridges [*Forsyth et al.*, 2002; *Forsyth*, 2004] have a rather random age progression (although often with a clear trend [*Lynch*, 1999]), and small-scale convection has been suggested as a possible mechanism to explain those ridges. Those chains all align roughly with the present-day plate motion direction, and comparing their age with the age of the HEB gives us an upper limit for the realignment period. Most of these ridges are significantly younger than the suggested 43–47 age of the HEB, but even those ridges suggest that realignment does not take longer than around 40 Ma. The Crossgrain ridges sit on 60–80 Ma seafloor and their actual age range could be close to that of the HEB [*Lynch*, 1999]. The Crossgrain ridges have propagated roughly from west to east, and at their most western, and probably oldest end, they blend into the more N-S oriented Line Islands. This suggests an even shorter realignment period than predicted by our calculations, and may suggest the need for a thin asthenosphere as well as

a non-Newtonian rheology. Although precise age measurements are not available yet, future improvements in this direction may provide some useful evidence for the formation date of the ridges with respect to the HEB timing.

[28] Another line of evidence to further constrain our rheological parameter space may be the presence of seismic anisotropy. Several studies indicate that the amplitude of seismic anisotropy in the old Pacific is small compared to that in the young Pacific [*Nishimura and Forsyth*, 1989; *Becker et al.*, 2003; *Smith et al.*, 2004]. The seismic anisotropy arising from shearing below the young Pacific plate motion might be partly destroyed by the appearance of SSC under older oceanic lithosphere. Regular SSC rolls might change, but not necessarily completely destroy large-scale anisotropy. But some of our calculations also show rather chaotic convection, in which anisotropy would probably be completely random in small length scales, and therefore canceling on the larger length scales at which anisotropy is measured. Our results show that, after a change in relative plate motion direction, the roll structure changes from a rather regular pattern of parallel roll structures to a more chaotic pattern for several tens of Ma. If conditions are favorable, a new regular roll pattern emerges afterward. We hypothesize that regular SSC might still be able to preserve or newly create seismic fabric, but that especially during this chaotic realignment phase, any present fabric might be destroyed. Furthermore, maps of seismic anisotropy suggest that the oldest parts of the Pacific lithosphere have a preferred orientation of the seismic velocities that in the shallow portions of the plate align with the (frozen-in) paleo-spreading direction at shallow depth, and in the deeper portions tend to align with the present-day plate motion in deeper portions of the lithosphere [*Nishimura and Forsyth*, 1989; *Smith et al.*, 2004]. If this anisotropy was formed by SSC at the bottom of the lithosphere, the depth of anisotropy may be related to a thickness of the lithosphere at the time of fabric formation, and thus a lithospheric age, which might give us more information on the orientation of SSC through time for this part of the lithosphere. Further modeling studies are being performed to quantify the evolution of seismic anisotropy in the presence of SSC.

5. Conclusions

[29] SSC rolls tend to align with plate motion, and a sudden change in relative plate motion direction would have an influence on the roll structure. Understanding the development of these SSC rolls after such event is important for our understanding of possibly related processes such as gravity lineations and some intraplate volcanic chains. We investigated the influence of a change in the relative plate motion on the presence, style, and realignment pattern of small-scale convection. In particular, we focused on the role of rheology. Our model results show that complete realignment of roll structures with the new plate motion direction can be expected within 20 Ma, but might also take much longer, depending on the rheological parameters. The most important influence on the realignment period is the shear force from both large-scale shear between the lithosphere and the deeper mantle, and small-scale shear created by the SSC itself. The realignment period is inversely correlated to the total shear, and therefore positively correlated to the thickness of the shear layer and the vigor of SSC, and negatively correlated to the relative plate velocity. Dislocation creep rheology reorientation takes much less time than with diffusion creep rheology, because shear rates are much higher in the first case. Unlike in the onset time, scale and vigor of SSC [e.g., *Huang et al.*, 2003; *van Hunen et al.*, 2005], the activation energy E^* plays a very minor role in the realignment phase, because it does not significantly influence the shear rates.

Acknowledgments

[30] Two reviewers (Caroline Dumoulin and Garrett Ito), associate editor Magali Billen, and editor Peter van Keken are thanked for their many good suggestions to improve the manuscript. JvH would like to thank Jean-Paul (Pablo) Ampuero for fruitful discussions. SZ is supported by David and Lucile Packard Foundation and National Science Foundation grants EAR 0134939 and EAR 0409217.

References

Becker, T. W., J. B. Kellog, G. Ekström, and R. J. O'Connell (2003), Comparison of azimuthal seismic anisotropy from surface waves and finite strain from global mantle-circulation models, *Geophys. J. Int.*, *155*, 696–714.

Brooks, A. N., and T. J. R. Hughes (1982), Streamline upwind/Petrov-Galerkin formulations for convection dominated flows with particular emphasis on the incompressible Navier-Stokes equations, *Comput. Methods Appl. Mech. Eng.*, *32*, 199–259.

Buck, W. R., and E. M. Parmentier (1986), Convection beneath young oceanic lithosphere: Implications for thermal structure and gravity, *J. Geophys. Res.*, *91*, 1961–1974.

Choblet, G., and C. Sotin (2000), 3D thermal convection with variable viscosity: Can transient cooling be described by a quasi-static scaling law?, *Phys. Earth Planet. Inter.*, *119*, 321–336.

Christensen, U. R. (1984), Convection with pressure and temperature dependent non-Newtonian rheology, *Geophys. J.R. Astron. Soc.*, *77*, 242–284.

Davaille, A., and C. Jaupart (1994), Onset of thermal convection in fluids with temperature-dependent viscosity: Application to the oceanic mantle, *J. Geophys. Res.*, *99*, 19,853–19,866.

Doin, M.-P., and L. Fleitout (1996), Thermal evolution of the oceanic lithosphere: An alternative view, *Earth Planet. Sci. Lett.*, *142*, 121–136.

Dumoulin, C., M.-P. Doin, D. Arcay, and L. Fleitout (2005), Onset of small-scale instabilities at the base of the lithosphere: Scaling laws and role of pre-existing lithospheric structures, *Geophys. J. Int.*, *160*, 344–356.

Feng, X., and P. Milanfar (2002), Multiscale principal components analysis for image local orientation estimation, paper presented at 36th Asilomar Conference on Signals, Systems and Computers, Inst. of Electr. and Electron. Eng., Pacific Grove, Calif.

Forsyth, D. (2004), On the origin of non-hotspot, intraplate volcanic ridges and gravity lineations, with constraints from the GLIMPSE experiment, *Eos Trans. AGU*, *85*(28), West. Pac. Geophys. Meet. Suppl., Abstract T12A-03.

Forsyth, D., S. Webb, D. Scheirer, C. Langmuir, R. Duncan, and K. Donnely (2002), COOK16MV cruise report R/V Melville; Tahiti-Easter i., technical report, Brown Univ., Providence, R. I.

Hager, B. H., and M. A. Richards (1989), Long wavelength variation in Earth's geoid: Physical models and dynamical implications, *Philos. Trans. R. Soc. London, Ser. A*, *328*, 309–327.

Haxby, W. F., and J. K. Weissel (1986), Evidence for small-scale mantle convection from SEASAT altimetry data, *J. Geophys. Res.*, *91*, 3507–3520.

Houseman, G. A., and D. P. McKenzie (1982), Numerical experiments on the onset of convective instability in the Earth's mantle, *Geophys. J.R. Astron. Soc.*, *68*, 133–164.

Howard, L. N. (1964), Convection at high Rayleigh number, in *Proceedings of the 11th International Congress on Applied Mechanics*, edited by H. Gortler, pp. 1109–1115, Springer, New York.

Huang, J., and S. Zhong (2005), Sublithospheric small-scale convection and its implications for the residual topography at old ocean basins and the plate model, *J. Geophys. Res.*, *110*, B05404, doi:10.1029/2004JB003153.

Huang, J., S. Zhong, and J. van Hunen (2003), Controls on sublithospheric small-scale convection, *J. Geophys. Res.*, *108*(B8), 2405, doi:10.1029/2003JB002456.

Karato, S.-i., and P. Wu (1993), Rheology of the upper mantle: A synthesis, *Science*, *260*, 771–778.

Katzman, R., L. Zhao, and T. H. Jordan (1998), High-resolution, two-dimensional vertical tomography of the central Pacific mantle using ScS reverberations and frequency-dependent travel times, *J. Geophys. Res.*, *103*, 17,933–17,971.

Korenaga, J., and T. H. Jordan (2003), Physics of multiscale convection in Earth's mantle: Onset of sublithospheric convection, *J. Geophys. Res.*, *108*(B7), 2333, doi:10.1029/2002JB001760.

Lynch, M. A. (1999), Linear ridge groups: Evidence for tensional cracking in the Pacific plate, *J. Geophys. Res.*, *104*, 29,321–29,333.

Marquart, G. (2001), On the geometry of mantle flow beneath drifting lithospheric plates, *Geophys. J. Int.*, *144*, 356–372.

McKenzie, D. P., J. M. Roberts, and N. O. Weiss (1974), Convection in the mantle: Towards a numerical simulation, *J. Fluid Mech.*, *62*, 465–538.

Morency, C., M.-P. Doin, and C. Dumoulin (2005), Three-dimensional numerical simulations of mantle flow beneath mid-ocean ridges, *J. Geophys. Res.*, *110*, B11407, doi:10.1029/2004JB003454.

Moresi, L., and M. Gurnis (1996), Constraints on the lateral strength of slabs from three-dimensional dynamic flow models, *Earth Planet. Sci. Lett.*, *138*, 15–28.

Moresi, L., and V. S. Solomatov (1995), Numerical investigation of 2D convection with extremely large viscosity variations, *Phys. Fluids*, *7*(9), 2154–2162.

Morgan, W. J. (1971), Convection plumes in the lower mantle, *Nature*, *230*, 42.

Nagihara, S., C. R. B. Lister, and J. G. Sclater (1996), Reheating of old oceanic lithosphere: Deductions from observations, *Earth Planet. Sci. Lett.*, *139*, 91–104.

Nishimura, C. E., and D. W. Forsyth (1989), The anisotropic structure in the upper mantle of the Pacific, *Geophys. J.*, *94*, 479–501.

Parsons, B., and D. McKenzie (1978), Mantle convection and thermal structure of the plates, *J. Geophys. Res.*, *83*, 4485–4496.

Raddick, M. J., E. M. Parmentier, and D. S. Scheirer (2002), Buoyant decompression melting: A possible mechanism for intraplate volcanism, *J. Geophys. Res.*, *107*(B10), 2228, doi:10.1029/2001JB000617.

Richter, F. M. (1973), Convection and large-scale circulation of the mantle, *J. Geophys. Res.*, *78*, 8735–8745.

Richter, F. M., and B. Parsons (1975), On the interaction of two scales of convection in the mantle, *J. Geophys. Res.*, *80*, 2529–2541.

Rieger, B., and L. J. van Vliet (2003), Representing orientation in n-dimensional spaces, *Lecture Notes Comput. Sci.*, *2756*, 17–24.

Ritzwoller, M. H., N. M. Shapiro, and S. Zhong (2004), Cooling history of the Pacific lithosphere, *Earth Planet. Sci. Lett.*, *226*, 69–84.

Schubert, G., D. L. Turcotte, and P. Olson (2001), *Mantle Convection in the Earth and Planets*, Cambridge Univ. Press, New York.

Searle, R., J. Francheteau, and B. Cornaglia (1995), New observations on mid-plate volcanism and the tectonic history of the Pacific plate, Tahiti to Easter Microplate, *Earth Planet. Sci. Lett.*, *131*, 395–421.

Smith, D. B., M. H. Ritzwoller, and N. M. Shapiro (2004), Stratification of anisotropy in the Pacific upper mantle, *J. Geophys. Res.*, *109*, B11309, doi:10.1029/2004JB003200.

Solomatov, V. S. (1995), Scaling of temperature- and stress-dependent viscosity convection, *Phys. Fluids*, *7*, 266–274.

Solomatov, V. S., and L. N. Moresi (2000), Scaling of time-dependent stagnant convection: Application to small-scale convection on Earth and other terrestrial planets, *J. Geophys. Res.*, *105*, 21,795–21,817.

Steinberger, B., R. Sutherland, and J. O'Connell (2004), Prediction of Emperor-Hawaii seamount locations fom a revised model of global plate motion and mantle flow, *Nature*, *430*, 167–173.

Tarduno, J. A., et al. (2003), The Emperor seamounts: Southward motion of the Hawaiian hotspot plume in Earth's mantle, *Science*, *301*, 1064–1069.

Turcotte, D. L., and G. Schubert (2002), *Geodynamics: Applications of Continuum Physics to Geological Problems*, 2nd ed., Cambridge Univ. Press, New York.

van Hunen, J., J. Huang, and S. Zhong (2003), The effect of shearing on the onset and vigor of small-scale convection in a Newtonian rheology, *Geophys. Res. Lett.*, *30*(19), 1991, doi:10.1029/2003GL018101.

van Hunen, J., S. Zhong, N. M. Shapiro, and M. H. Ritzwoller (2005), New evidence for dislocation creep from 3-D geodynamic modeling of the Pacific upper mantle structure, *Earth Planet. Sci. Lett.*, *238*, 146–155.

Zhong, S., M. T. Zuber, L. Moresi, and M. Gurnis (2000), Role of temperature-dependent viscosity and surface plates in spherical shell models of mantle convection, *J. Geophys. Res.*, *105*(B8), 11,063–11,082.